Mechanistic insights into solution-phase

oxidative esterification of primary alcohols on

Pd(111) from first-principles microkinetic

modeling

Eric D. Hermes, Aurora N. Janes, and J.R. Schmidt\*

Department of Chemistry and Theoretical Chemistry Institute, University of

Wisconsin-Madison, 1101 University Ave., Madison, WI 53706, United States

E-mail: schmidt@chem.wisc.edu

Abstract

We present an ab initio microkinetic model for the oxidative esterification of 1-

propanol to methyl propionate over Pd(111). The model fully accounts for solvation

of solution-phase species and added catalytic base, and provides key insights into the

factors which limit the activity of unpromoted Pd aerobic oxidation catalysts. In par-

ticular, we find that activity is limited by the large steady state surface H coverage,

which destabilizes other adsorbed intermediates via lateral interactions, and substantial

barriers governing the formation of O-H bonds, which is required for the reduction of

 $\mathcal{O}_2$  and removal of H by products from the catalyst surface.

**Keywords** 

density functional theory, microkinetic modeling, palladium, catalysis, dehydrogenation, es-

terification, alcohol oxidation

1

### 1 Introduction

Selective oxidation of alcohols to carbonyl compounds is an important class of chemical transformations used in a wide variety of synthetic applications ranging from pharmaceuticals to industrial-scale bulk chemicals. Aldehydes and esters, in particular, are highly valued for both their intrinsic properties and as reagents in other synthetic pathways. These compounds are typically accessed through oxidation of their alcohol analogues, frequently via stoichiometric reaction with an oxidizing agent in transformations which are both inefficient and generate a substantial amount of byproduct. Heterogeneous catalysis provides an alternative route for the selective oxidation of alcohols using molecular oxygen, which improves both efficiency and prospects for scale-up.

While pure platinum group metals (PGM) such as Pt and Pd are capable of catalyzing the aqueous-phase aerobic oxidation of alcohols,<sup>5</sup> catalyst activity can be greatly improved via addition of promoters, such as Bi, Te, or Pb. 6-9 Promoters are especially useful in the oxidative dehydrogenation of aliphatic primary alcohols, which typically exhibit poor yields in the absence of main group promoters. 10 Although the mechanism of action of the promoters is unknown, a number of hypotheses have been put forth. 11-16 Furthermore, it has been shown that metallic (rather than oxidized) PGM sites are responsible for the bulk of catalytic activity in these systems. 17-22 Experimental measurements of Pt metal catalyst working potentials indicate that the catalyst becomes reduced upon exposure to the alcohol substrate relative to the oxidized air-exposed resting catalyst. 16,23 Moreover, cyclic voltammetry experiments show that Bi-promotion, which improves catalyst activity, suppresses H sorption on Pt catalysts, which indicates a negative correlation between surface H coverage and catalyst activity. 16 These observations suggest that unpromoted catalysts are likely at least partially hydrogen-covered under operating conditions, in contrast to the partially oxygen-covered resting (air-exposed) catalyst. 10,16 Further characterization of these catalysts is complicated by the difficulty of performing in situ measurements of liquid-phase heterogeneous catalysts.

The exact mechanism for the oxidative esterification of primary alcohols over PGM is

a matter of some debate. For at least some alcohols, such as benzyl alcohol, an aldehyde intermediate can be isolated. In contrast, for other alcohols such as 1-octanol, the aldehyde intermediate either reacts too rapidly to be detected, or does not form at all. The exact process by which the aldehyde forms is not known. Under basic conditions, it has been proposed that the alcohol becomes deprotonated in solution and undergoes hydride elimination on the catalyst surface to form the aldehyde. This hypothesis has been disputed due to the observation that oxidation also occurs under acidic conditions, and it has been proposed instead that the alkoxide is formed on the catalyst surface. And it has been suggested that it is the C-H bond that is broken first due to its weaker bond strength.

The subsequent oxidation of aldehyde to ester is also poorly understood. The aldehyde intermediate may desorb from the surface and react with alcohol in solution to form a hemi-acetal species. The putative hemiacetal intermediate must be further dehydrogenated to the final ester product, analogous to the initial dehydrogenation of the alcohol to the aldehyde. However, such an aldehyde intermediate cannot always be identified, suggesting that alternative pathways may also exist. Consequently, the detailed aldehyde esterification mechanism is also highly non-trivial.

In a prior computational work, Hibbitts and Neurock suggest various pathways for the dehydrogenation and oxidation of ethanol to acetate based on the DFT-calculated energetics and barrier heights for a series of reactions on the water-solvated Pd(111) surface.<sup>35</sup> However, due to the complexity of their setup, they were unable to perform a full microkinetic analysis, and thus their conclusions regrading the predominant reaction pathways relied upon assumptions about the condition of the working catalyst surface (e.g. hydrogen coverage).

In this work, we use Pd(111)-catalyzed esterification of 1-propanol to methyl propionate under basic conditions as a model of aliphatic primary alcohol esterification. We utilize first-principles microkinetic modeling informed by density functional theory (DFT) calculations of the catalyst surface and the solution-phase species. Microkinetic analysis of the reaction network allows us to identify the dominant reaction pathways that contribute to the catalytic

activity from the large number of possible routes from propanol to the final ester product. It also facilitates a direct examination of the state of the catalyst under working conditions and the role of various reactants, including, in particular, the role of catalytic base.

In order to achieve these goals, we develop several novel microkinetic modeling techniques for the analysis of liquid-phase heterogeneous catalytic reaction networks. This work is one of the first comprehensive application of first-principles microkinetic modeling to a liquid-phase heterogeneous reaction network containing charged reactants, accounting for the effects of solvation on both thermodynamics and mass transport. Additionally, we introduce a method to account for adsorption and desorption of charged reactants and their influence on subsequent adsorption / reaction. Interestingly, while we find intermediate and transition state energies for our system that are in qualitative agreement with the prior findings of Hibbitts and Neurock, the predominant reaction pathways differ, likely due to the strong influence of the catalysts surface coverage under steady-state working conditions, thus highlighting the importance a detailed microkinetic model for this reaction network.

## 2 Theoretical methods

The energies and geometries of surface-bound species were determined with the periodic density functional theory (DFT) code VASP in a basis of plane waves up to a cutoff energy of 450 eV. 36–39 All calculations were run using the Python environment ASE. 40 Geometry optimizations and vibrational frequency calculations were performed with the PBE-D3(ABC) dispersion-corrected density functional method, and single-point energies were evaluated with the range-separated HSE06-D3(BJ,ABC) method at the PBE-D3(ABC) geometries. 41–51 While DFT calculations using hybrid functionals such as HSE06 are significantly more computationally expensive than typical semilocal functionals such as PBE, the inclusion of exact exchange has a substantial effect on reaction barrier heights and intermediate binding energies. 52–54 PBE-D3(ABC) yields a lattice constant of 3.90 Å for bulk

Pd, which compares favorably to the experimental lattice constant of 3.89 Å.<sup>55</sup> The Pd(111) surface was modeled as a 4-layer 3x3 slab with a 15 Å vacuum gap, and the Brillouin zone was sampled with a 3x3x1 Monkhorst-Pack k-point mesh.<sup>56</sup> The bottom two layers of the slab were fixed to the PBE-D3(ABC) lattice constant, while the top two layers were allowed to relax in all geometry optimizations. The effect of solvation on the catalyst surface and adsorbed intermediates were included through the use of single-point GLSSA13 continuum solvation model calculations using VASPsol with methanol as the solvent at the PBE level of theory.<sup>57–59</sup> Pathways for all reactions were located using the nudged elastic band method, <sup>60–62</sup> and transition states were optimized using the dimer method. <sup>45,63,64</sup> All transition states were verified to have exactly one imaginary vibrational frequency corresponding to the expected reaction coordinate.

Solution-phase species were optimized in Gaussian 09<sup>65</sup> with the PBE-D3(ABC) method using the aug-cc-pVTZ basis set <sup>66</sup> and the SMD continuum solvation model <sup>67</sup> with methanol solvent. SMD was chosen since it was parameterized to reproduce experimental total free energies of solvation, including the cavitation energy. Note that for periodic calculations involving the catalyst surface, the GLSSA13 PCM is used instead of SMD. This is because SMD is parameterized to reproduce experimental free energies of solvation, which includes contributions arising from the loss of translational entropy of gas-phase species. This is not relevant for immobile systems, such as adsorbates on the catalyst surface. Similarly, GLSSA13 would predict inaccurate solvation free energies of species in solution due to its neglect of translational entropy loss. Single-point calculations were performed with the HSE06-D3(BJ,ABC) method<sup>51</sup> and the resulting energies were extrapolated to the complete basis set limit using the aug-cc-PVnZ basis sets (n = 2 to 5). Calculations were performed with and without solvation correction to determine the free energy of solvation, which was used to correct the energy of the gas-phase species as determined in VASP (see Figure 1). Additionally, the energy of species that carry a formal negative charge was determined by performing calculations of the corresponding neutral radical in VASP, and adding to that the electron affinity of that species as determined in Gaussian.

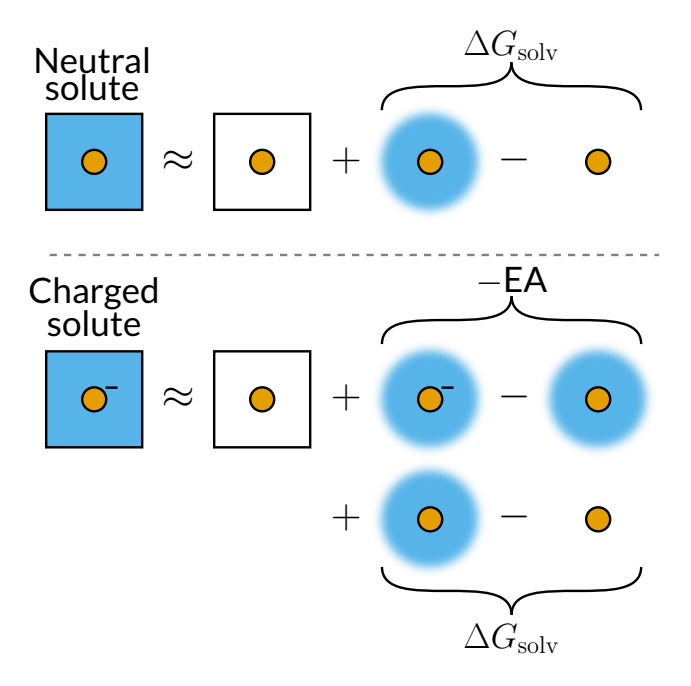


Figure 1: Schematic illustration of energy calculations for solution-phase species. The energy of a species in solution under periodic boundary conditions is approximated as the energy of the species in the absence of solvation under periodic boundary conditions plus the free energy of solvation, which is determined using Gaussian and SMD. For anions, we calculate the energy of the corresponding neutral radical under periodic boundary conditions without solvation, then add both the electron affinity and the solvation free energy determined using Gaussian and SMD.

The reaction network was analyzed using the Micki package, <sup>68</sup> which allows for the construction and solution of microkinetic models from *ab initio* calculations. On-surface reaction rate constants were calculated using transition state theory. Reverse rate constants were chosen such that all reactions obey detailed balance. For barrierless on-surface reactions, transition state theory was used with a free energy barrier of 0 eV in the exothermic direction, resulting in a rate constant of  $k_BT/h$ . We treat  $O_{2(g)}$  as a gas phase species and enforce its equilibrium surface converage. This is because  $O_2$  has a low solubility in methanol and is typically introduced to the system by bubbling gas through the reactor. The rate of adsorption of all solution-phase species were calculated using a Langmuir equilibration-diffusion model (see Figure 2), which is described in detail in the SI. This model for the rate of diffusion-

limited adsorption is similar to one developed by Hansen, Viswanathan, and Nørskov. <sup>69</sup> For all simulations, a stationary layer thickness of 100 µm was used for diffusion. This choice of length scale motivated by a model for the laminar creeping flow of solvent around a spherical nanoparticles with a diameter of 1 nm.

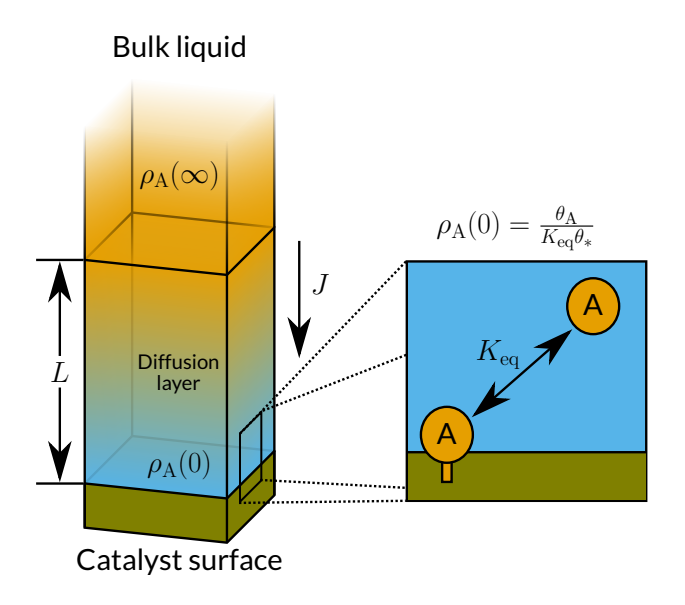


Figure 2: Schematic illustration of diffusion-limited adsorption model. Species A is represented by the color orange, and solvent (i.e. methanol) is represented by the color blue. L is the diffusive layer thickness,  $\rho_{\rm A}(\infty)$  is the concentration of species A in the bulk solution,  $\rho_{\rm A}(0)$  is the concentration of species A in the layer of solution that is in direct contact with the catalyst surface, J is the net flux of species A towards the catalyst surface,  $K_{\rm eq}$  is the equilibrium constant for the adsorption of species A to the catalyst surface,  $\theta_{\rm A}$  is the coverage of species A on the catalyst surface, and  $\theta_*$  is the fractional number of unoccupied sites on the catalyst surface.

The free energies of adsorbates were calculated by treating all molecular degrees of freedom under the harmonic oscillator approximation. Vibrations involving metal atoms were omitted from the analysis.  $O_{2(g)}$  was treated as an ideal gas. The free energies of solutionphase species were calculated by adding the free energy of solvation determined by the SMD continuum solvation model to the free energy of the species in the gas-phase determined with the ideal gas approximation. This procedure results in an accurate approximation to the absolute free energy of the solution-phase species. The reference state of  $O_{2(g)}$  and all solution-phase species was chosen to be 1 M, which is the standard state for solutionphase species. Note that this choice affects the reported free energy of adsorption, but does not affect any thermodynamic or kinetic parameters of the model. A diffusion constant of  $2 \times 10^{-9} \,\mathrm{m}^2/\mathrm{s}$  was used for all solution-phase species. We find that while adsorption is diffusion-limited, it is not rate limiting, and as such the results of our microkinetic model are invariant to the choice of diffusion constant to within an order of magnitude for all species.

We assume that the base reacts with the solvent (methanol) quantitatively to form methoxide, and we ignore the presence of any resulting conjugate acid. In this way, we control the concentration of the base by changing the concentration of methoxide in solution. We further set the concentration of the propoxide anion in solution to obey the predicted equilibrium for proton transfer from propanol to methoxide.

For adsorption of anions to the catalyst surface, we assume that the electron is transferred from the anion to the metal, resulting in a change in energy that depends on the work function of the metal. To account for a buildup of charge on the catalyst, we introduce an electron-electron repulsion energy that further modulates the binding energy of anions. This electron-electron repulsion energy corresponds to the differential energy of introducing charge to a capacitor, as a charged surface forms a double-layer capacitor in solution with counterions, which accumulate near the surface. A more detailed discussion on our double-layer capacitor model can be found in the SI.

Both PBE-D3(ABC) and HSE06-D3(BJ,ABC) predict the dissociative adsorption of  $H_2$  to Pd(111) to be substantially more exothermic than experiments have shown. Consequently, the energy of surface-bound hydrogen atoms was offset by a constant value to accurately match the experimental binding enthalpy measured by Silbaugh and Campbell.<sup>70</sup>

The binding energy of all stable intermediates were also calculated on an H-saturated surface with a single hydrogen atom removed to make room for the adsorbate. The resulting binding energy was used to construct a linear dependence of the binding energy of all intermediates to the H coverage. Similar calculations were done to determine the lateral

self-interactions of O and  $O_2$ . The lateral self-interactions of H, O, and  $O_2$  were fitted to

$$E(\operatorname{slab} + nX) - E(\operatorname{slab}) = nE(\operatorname{slab} + X) + \frac{n^2}{m}E(X \cdot \cdot \cdot X), \tag{1}$$

where E(slab + X) is the energy of X on the surface at infinite dilution, m is the number of binding sites in the periodic slab model (in our model, m = 9), and  $E(X \cdot \cdot \cdot X)$  are the mean-field lateral interactions of species X with itself. We fit the zero-coverage energy and lateral interaction energies of H, O, and  $O_2$  by solving this equation exactly for n = 1 and n = 9. For the lateral interaction of other species with H, we solve a similar equation,

$$E(\operatorname{slab} + \operatorname{X} + n\operatorname{H}) - E(\operatorname{slab}) - nE(\operatorname{slab} + \operatorname{H}) - \frac{n^2}{m}E(\operatorname{H} \cdots \operatorname{H}) = E(\operatorname{slab} + \operatorname{X}) + \frac{n}{m}E(\operatorname{H} \cdots \operatorname{X}). \tag{2}$$

This equation is solved exactly for n = 0 and n = 8.

Corrections to the free energy of transition states were calculated as

$$\Delta E_{\rm ts} = \alpha \Delta E_{\rm prod} + (1 - \alpha) \Delta E_{\rm react}, \tag{3}$$

where  $\Delta E_i$  is the correction to the free energy of species *i* including lateral interactions effects, and  $\alpha$  is the lateness of the transition state, which we approximate as

$$\alpha = \frac{\Delta G_{\text{for}}^{\ddagger}}{\Delta G_{\text{for}}^{\ddagger} + \Delta G_{\text{rev}}^{\ddagger}},\tag{4}$$

where  $\Delta G^{\ddagger}$  is the forward or reverse free energy barrier *excluding* coverage effects. If a species includes a constant correction to the free energy (such as adsorbed H, to match experimental values), equations 3 and 4 are solved self-consistently.

The reactor was modeled as an idealized continuous stirred-tank reactor (CSTR) at 330 K.

The gas- and solution-phase concentration of all reactants and products were fixed to their initial values. The coupled differential equations were solved until the rate of change of all

concentrations and coverages was less than  $1 \times 10^{-6} \,\mathrm{s}^{-1}$ . Sensitivity analysis was performed by numerically perturbing model parameters and re-running the model to find the new steady state conditions. For each reaction, Campbell's degree of rate control ( $\chi_{RC}$ ) was determined by increasing and decreasing the forward and reverse rate constants by 0.1%. For each species, the thermodynamic rate control ( $\chi_{TRC}$ ) was determined by increasing and decreasing the free energy of the species by  $0.001k_BT$ . The effective activation barrier of the model was determined by increasing and decreasing the reactor temperature by  $0.01 \,\mathrm{K}$ .

Note that our definition of the degree of thermodynamic rate control differs from the definition given by Campbell in which the free energy of all other species and all transition states are kept fixed. This is because in our microkinetic model, the energy of a transition state depends on the energy of the reactants and products of reactions that pass through that transition state. For a more thorough discussion of our sensitivity analysis implementation, see the SI.

## 3 Results and Discussion

### 3.1 DFT results

Reaction free energies and barriers were calculated for all plausible elementary steps for the oxidative esterification of propanol to methyl propionate. A subset of these energies under steady state (those found to be kinetically relevant, vide infra) are given in Table 1; a comprehensive listing of all considered reactions and the corresponding DFT-calculated results for both the pristine and steady-state surface can be found in the SI.

The free energies of reaction and barrier heights on the pristine surface are in qualitative agreement with the results of Hibbitts and Neurock<sup>35</sup> (pristine results not shown here, see table S3). In particular, we find that oxygen assistance greatly lowers the barrier to cleavage of O-H bonds, but not C-H bonds (these reactions are omitted from Table 1 in the main text, as they are not found to be kinetically relevant). Similarly, we find dehydrogenation

Table 1: Free energies of reaction and forward and reverse free energy barriers for the reactions found to be relevant in the microkinetic model (discussed later) under steady state conditions. Results for all reactions considered in our model under both pristine and steady state conditions can be found in the SI. Missing values for  $\Delta G_{\text{for}}^{\ddagger}$  and  $\Delta G_{\text{rev}}^{\ddagger}$  indicate that the reaction is barrierless.

Reaction	$\Delta G \text{ (eV)}$	$\Delta G_{\mathrm{for}}^{\ddagger} \; (\mathrm{eV})$	$\Delta G_{\rm rev}^{\ddagger} \; ({ m eV})$
$RCH_2OH_{(sol'n)} + * \longleftrightarrow RCH_2OH*$	-0.01	242	
$RCH_2O_{(sol'n)} + * \longleftrightarrow RCH_2O * + e^-$	0.44		
$CH_3O_{(sol'n)}^{-} + * \longleftrightarrow CH_3O^* + e^-$	0.34		
$O_{2(g)} + * \longleftrightarrow O_2 *$	0.24		
$RCH_2OH* + OH* \longleftrightarrow RCH_2O* + H_2O*$	-0.06		
$RCH_2OH* + * \longleftrightarrow RCHOH* + H*$	0.25	0.81	0.56
$RCH_2O* + * \longleftrightarrow RCHO* + H*$	-0.92	0.27	1.20
$RCHOH* + O_2* \longleftrightarrow RCHO* + OOH*$	-0.06		
$  \text{RCHO}* \longleftrightarrow \text{RCHO}_{(\text{sol'n})} + * $	-0.03		
$RCHO* + * \longleftrightarrow RCO* + H*$	-0.04	0.22	0.26
$RCO* + CH_3O* \longleftrightarrow RCOOCH_3* + *$	-1.89	0.08	1.77
$  \operatorname{RCHO}_{(\operatorname{sol'n})} + \operatorname{CH}_3 \operatorname{O}_{(\operatorname{sol'n})}^- \longleftrightarrow \operatorname{RCHOOCH}_3^{(\operatorname{sol'n})}  $	-0.20		
$RCHOOCH_3^-$ (sol'n) $+* \longleftrightarrow RCHOOCH_3* + e^-$	0.36		
$RCHOOCH_3* + * \longleftrightarrow RCOOCH_3* + H*$	-1.51	0.30	1.81
$RCOOCH_3* \longleftrightarrow RCOOCH_{3(sol'n)} + *$	0.29		
$OOH* + * \longleftrightarrow O* + OH*$	-1.18	0.09	1.27
$OH* + e^- \longleftrightarrow OH^{(sol'n)} + *$	-0.75		
$H_2O*\longleftrightarrow H_2O_{(sol'n)}+*$	-0.22		
$CH_3O* + H* \longleftrightarrow CH_3OH* + *$	-0.86	0.47	1.33
$CH_3OH* + O* \longleftrightarrow CH_3O* + OH*$	0.23		
$CH_3OH* + OH* \longleftrightarrow CH_3O* + H_2O*$	-0.31		
$CH_3OH* \longleftrightarrow CH_3OH_{(l)} + *$	-0.11		
$2 H* \longleftrightarrow H_{2(sol'n)} + 2*$	0.49		

of propanol to form the hydroxypropyl intermediate is the most thermodynamically and kinetically favorable first step in the absence of surface oxygen species. In general, we find that most kinetically relevant steps in the model are exothermic and have small or no barriers, with the exception of the dehydrogenation of propanol to hydroxypropyl and the desorption of propanal and methyl propionate.

While Table 1 indicates that adsorption of anions is strongly disfavored, this is only the case under steady state conditions due to the buildup of excess negative charge on the catalyst surface. In fact, anions bind to the pristine surface very strongly, around 1.5 eV

to 2.0 eV, becoming less exothermic with increasing anion adsorption due to surface charge accumulation.

### 3.2 Microkinetic model results

Table 2: Steady state rates and degree of rate control for all reactions found to be relevant in the microkinetic model. Results for all reactions considered in our model can be found in the SI.

Reaction	Steady state rate $(h^{-1})$	Degree of rate control
$RCH_2OH_{(sol'n)} + * \longleftrightarrow RCH_2OH*$	95.6	0.000
$RCH_2O_{(sol'n)}^- + * \longleftrightarrow RCH_2O * + e^-$	-7.2	0.000
$CH_3O_{(sol'n)}^- + * \longleftrightarrow CH_3O^* + e^-$	105.1	0.000
$O_{2(g)} + * \longleftrightarrow O_2 *$	81.9	0.000
$RCH_2OH* + OH* \longleftrightarrow RCH_2O* + H_2O*$	13.7	0.000
$RCH_2OH* + * \longleftrightarrow RCHOH* + H*$	81.9	0.619
$RCH_2O* + * \longleftrightarrow RCHO* + H*$	6.5	-0.256
$RCHOH* + O_2* \longleftrightarrow RCHO* + OOH*$	81.9	0.005
$RCHO* \longleftrightarrow RCHO_{(sol'n)} + *$	46.8	-0.001
$RCHO* + * \longleftrightarrow RCO* + H*$	41.6	0.000
$RCO* + CH_3O* \longleftrightarrow RCOOCH_3* + *$	41.6	-0.001
$RCHO_{(sol'n)} + CH_3O_{(sol'n)}^- \longleftrightarrow RCHOOCH_3^{(sol'n)}$	46.8	0.000
$RCHOOCH_3^-$ (sol'n) $+* \longleftrightarrow RCHOOCH_3* + e^-$	46.8	0.000
$RCHOOCH_3* + * \longleftrightarrow RCOOCH_3* + H*$	46.8	-0.001
$RCOOCH_3* \longleftrightarrow RCOOCH_{3(sol'n)} + *$	88.4	-0.024
$OOH* + * \longleftrightarrow O* + OH*$	81.9	0.000
$OH* + e^- \longleftrightarrow OH^{(sol'n)} + *$	144.7	0.000
$H_2O*\longleftrightarrow H_2O_{(sol'n)}+*$	19.2	0.000
$CH_3O* + H* \longleftrightarrow CH_3OH* + *$	150.8	0.427
$CH_3OH* + O* \longleftrightarrow CH_3O* + OH*$	81.9	0.002
$CH_3OH* + OH* \longleftrightarrow CH_3O* + H_2O*$	5.4	0.000
$CH_3OH* \longleftrightarrow CH_3OH_{(l)} + *$	63.5	0.000
$2 H* \longleftrightarrow H_{2(sol'n)} + 2*$	12.9	0.452

Our microkinetic model yields an overall turnover frequency of about  $88.4 \,\mathrm{h^{-1}}$ , consistent with the low experimentally-observed activity of the unpromoted catalyst. Based on these results, we find that two pathways to the formation of methyl propionate contribute to the majority of the activity (see Table 2). The first pathway involves initial dehydrogenation of adsorbed propanol (RCH<sub>2</sub>OH) to hydroxypropyl (RCHOH), which reacts with adsorbed  $O_2$ 

Table 3: Steady state concentrations and degree of thermodynamic rate control for all adsorbates considered in our model.

Species	Steady state concentration	Thermodynamic rate control
Н	0.7352	-1.368
RCH <sub>2</sub> OH	0.1049	0.453
$RCOOCH_3$	0.0572	0.048
CH <sub>3</sub> OH	0.0376	0.182
RCHOHOCH <sub>3</sub>	< 0.0001	0.000
CH <sub>3</sub> O	< 0.0001	0.552
RCO	< 0.0001	-0.003
$O_2$	< 0.0001	0.010
RCHO	< 0.0001	-0.167
$RCHOOCH_3$	< 0.0001	-0.002
RCHOH	< 0.0001	0.769
$H_2O$	< 0.0001	0.000
О	< 0.0001	-0.005
$RCH_2O$	< 0.0001	-0.525
OOH	< 0.0001	0.002
OH	< 0.0001	0.005
$RCOHOCH_3$	< 0.0001	0.000
*	0.0650	

to form propanal (RCHO) and hydroperoxyl (OOH). OOH dissociates to O and hydroxyl (OH), and OH accepts an electron from the surface and leaves the catalyst as hydroxide (OH $^-$ ). Propanal desorbs from the surface and reacts in solution with methoxide to form a deprotonated hemiacetal anion (RCHOOCH $_3$  $^-$ ). This anion then adsorbs to the surface and undergoes  $\beta$ -hydride elimination to form methyl propionate (RCOOCH $_3$ ). The second pathway is identical up to the formation of propanal, at which point propanal becomes further dehydrogenated by the catalyst to propanoyl (RCO), which reacts with catalyst-bound methoxy to form methyl propionate. Both pathways contribute an essentially equal amount to the overall formation of methyl propionate (see Figure 7).

Since our microkinetic model accounts for lateral interactions between adsorbates, reaction energies and barrier heights depend on the catalyst surface coverage. In the discussion that follows, all reported energies correspond to the steady-state catalyst coverage. In general, this tends to raise barrier heights and destabilize intermediates that form strong bonds to the catalyst relative to that of the pristine catalyst. In particular, we find that the steady state catalyst has a large buildup of adsorbed H (see Table 3).

In the following sections, we will discuss the results of our microkinetic model by focusing on specific reactions that occur in the overall reaction network. We begin by discussing the dehydrogenation of propanal to propanal, followed by the esterification of propanal to form methyl propionate. We subsequently discuss the predominant pathway(s) by which H is removed from the catalyst surface, the reduction of  $O_2$  to form  $H_2O$ , and finally the role of catalytic base. We end by outlining the possible role of main-group element additives in promoting the dehydrogenation and oxidation of alcohols.

#### 3.2.1 Dehydrogenation of propanol to propanal

The first step towards formation of methyl propionate is the dehydrogenation of propanol to propanal. Formation of propanal involves sequential dehydrogenation at the alcohol oxygen and the adjacent carbon. These steps have different barriers depending on the order in which they occur, resulting in two possible pathways with different kinetics. We refer to the pathway in which the O-H bond is broken first as the "propoxy" pathway, and the pathway in which the C-H bond is broken first the "hydroxypropyl" pathway, after the partially dehydrogenated intermediates involved in the respective pathways.

In both pathways, we find that the barrier to O-H bond scission can be effectively eliminated by cooperative reduction of on-surface oxygen species in the form of O, OH, and O<sub>2</sub>. We do not find the same cooperativity for the C-H bond scission steps. While oxygen-assisted C-H bond scission can occur, in all cases we find these reactions to have a substantially higher free energy barrier than unassisted C-H bond scission. This is likely because the C-H bonds in the surface-bound intermediates in our model form agostic interactions with underlying Pd atoms, which facilitates C-H bond scission onto the catalyst surface (see Figure 3). In order for a coadsorbed oxygen species to abstract H directly from the C-H bond, this agostic interaction must be broken, which destabilizes the transition state

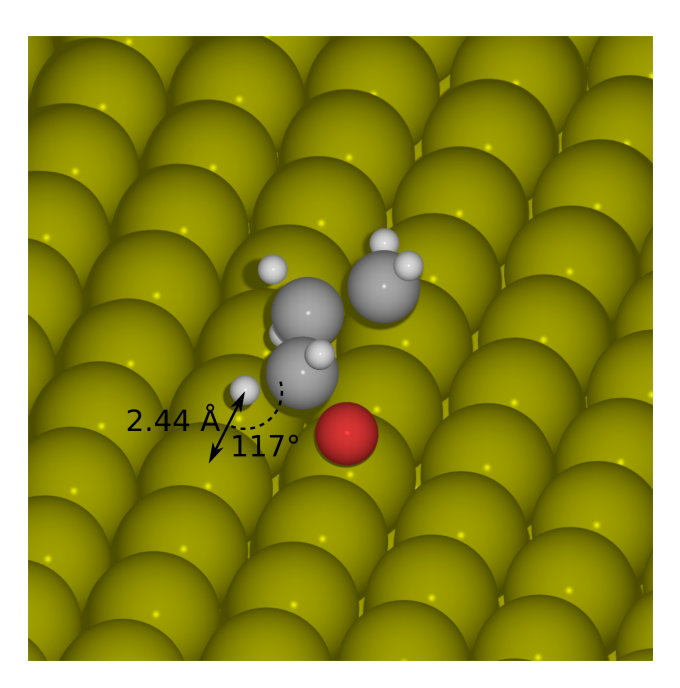


Figure 3: The propoxy intermediate adsorbed to the Pd(111) surface. The Pd-H distance and Pd-H-C angle are shown, which indicate an agostic type interaction.

relative to the unassisted mechanism. On the other hand, O—H bond containing species can form hydrogen bonds with coadsorbed oxygen species, which facilitates direct transfer of H from one oxygen atom to another.

In the propoxy pathway (see Figure 4), the initial unassisted O-H bond scission step has a free energy of reaction of  $1.10\,\mathrm{eV}$  and involves a substantial free energy barrier of  $1.64\,\mathrm{eV}$ . This reaction is made substantially more favorable via oxygen assistance, while also reducing the associated barriers. The barrier for C-H bond scission that occurs in the second step of the propoxy pathway has a free energy of reaction of  $-0.92\,\mathrm{eV}$  and a free energy barrier of  $0.27\,\mathrm{eV}$ .

The initial step of the hydroxypropyl pathway (see Figure 5) is C-H bond scission of adsorbed propanol, which has a free energy of reaction of 0.25 eV and a barrier of 0.81 eV. The second O-H bond scission step has a free energy of reaction of -0.07 eV and an unassisted barrier of 0.69 eV. Note that both steps of the hydroxypropyl pathway have similar free energy barriers, unlike the propoxy pathway, in which the barrier to unassisted O-H bond scission is substantially higher. As in the propoxy pathway, oxygen assistance eliminates

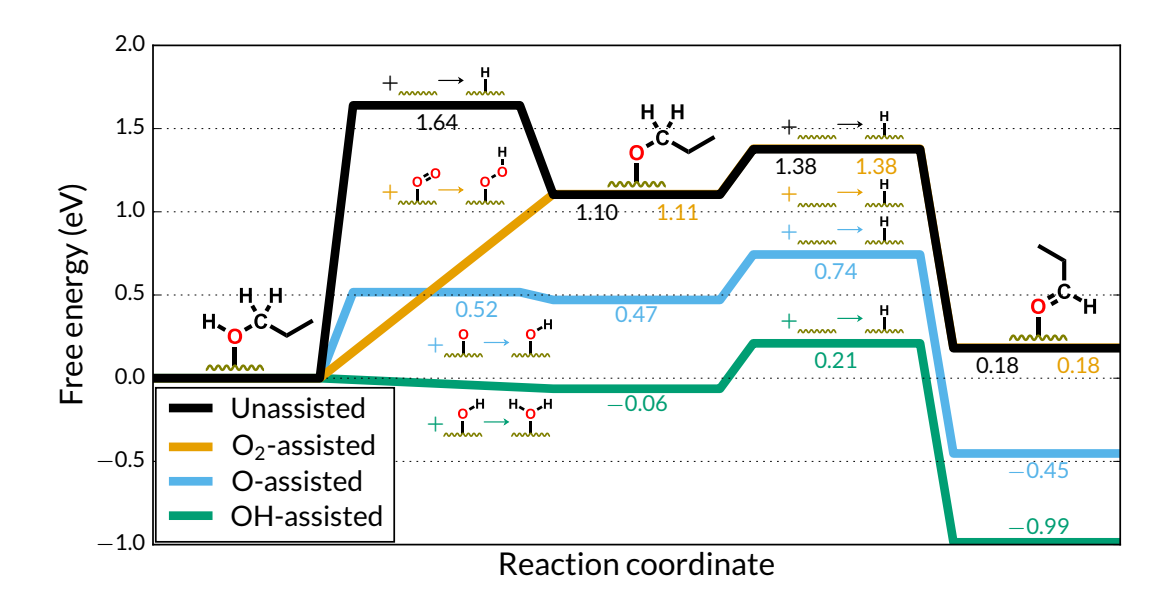


Figure 4: Free energy profile of the dehydrogenation of propanol to propanal through the adsorbed propoxy intermediate under steady state conditions via the unassisted (black), O<sub>2</sub>-assisted (orange), O-assisted (blue), and OH-assisted (green) mechanisms. The zero of free energy corresponds to all co-reactants separated but pre-adsorbed on the catalyst surface. The energetics of this pathway on the pristine surface are illustrated in Figure S2.

the barrier to O-H bond scission. While O-H bond scission of hydroxypropyl to propanal is exothermic in all cases, O-H bond scission of propanol to propoxy remains endothermic in most cases, with the exception of the OH-assisted mechanism, which is very slightly exothermic.

Based only on thermodynamic considerations, it is not a priori obvious which of these two pathways will predominate the catalyst's activity. It is clear that oxygen assistance lowers the barrier to O-H bond scission, and that the forward barriers are overall lower in the oxygen-assisted propoxy pathway. However, the kinetics of the reaction are governed both by the thermodynamics of the reactants and transition state and by the concentration of the reactants on the surface. In particular, the reaction of propanol (hydroxypropyl) with surface-bound O and OH is less endothermic (more exothermic) than reaction with surface-bound  $O_2$ . However, surface-bound O and OH are formed primarily by decomposition of surface-bound OOH (free energy barrier of  $0.09 \,\mathrm{eV}$ ), as the free energy barrier for  $O_2$ 

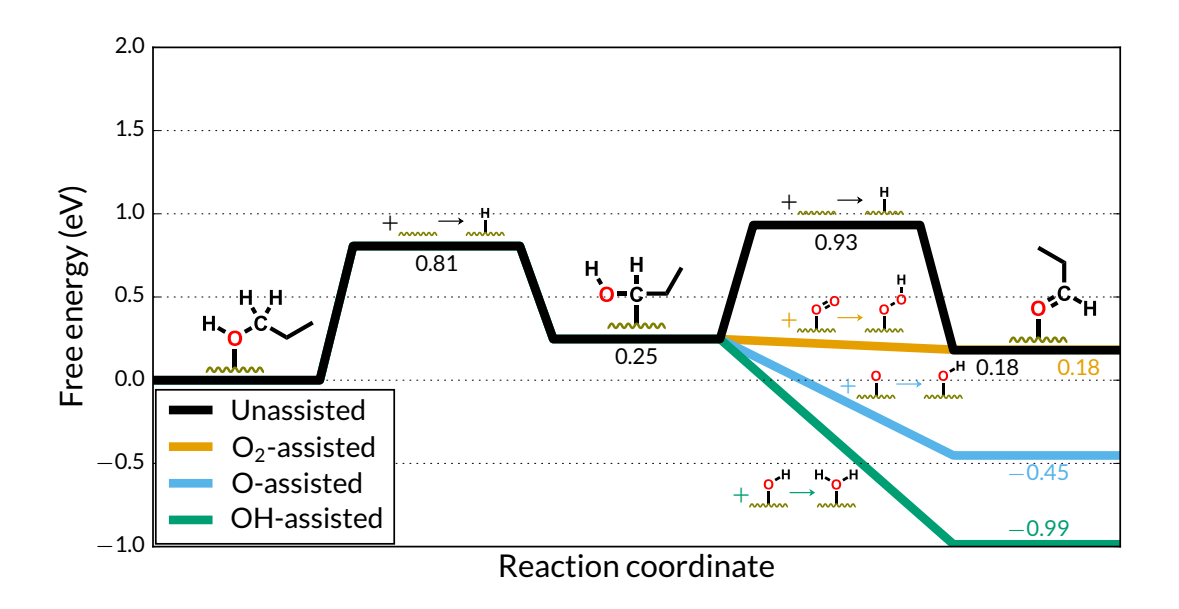


Figure 5: Free energy profile of the dehydrogenation of propanol to propanal through the adsorbed hydroxypropyl intermediate under steady state conditions via the unassisted (black), O<sub>2</sub>-assisted (orange), O-assisted (blue), and OH-assisted (green) mechanisms. The zero of free energy corresponds to all co-reactants separated but pre-adsorbed on the catalyst surface. The energetics of this pathway on the pristine surface are illustrated in Figure S3.

decomposition is a very substantial 1.24 eV. Moreover, formation of OOH by the purely onsurface reaction of  $O_2* + H*$  has a free energy barrier of 0.77 eV, which is more unfavorable than the endothermic reaction of  $O_2$  with propanol to form OOH and propoxide. This suggests that  $O_2$ -assisted O-H bond scission is a prerequisite for the O-assisted and OHassisted pathways, and therefore it must occur at some point in the reaction network.

Microkinetic modeling gives us the ability to identify which of the many plausible reaction pathways outlined above are, in fact, kinetically relevant. Based on our microkinetic model, we find that the initial dehydrogenation of propanol to form propanal proceeds largely through a single pathway: dehydrogenation of propanol to the hydroxypropyl intermediate, which reacts with coadsorbed  $O_2$  to form propanal and OOH (see Figure 6).

Initial dehydrogenation of propanol to the hydroxypropyl intermediate (via C-H bond cleavage) has the largest barrier and the highest degree of rate control of all elementary steps in the reaction network. This reaction is endothermic by 0.13 eV on the pristine

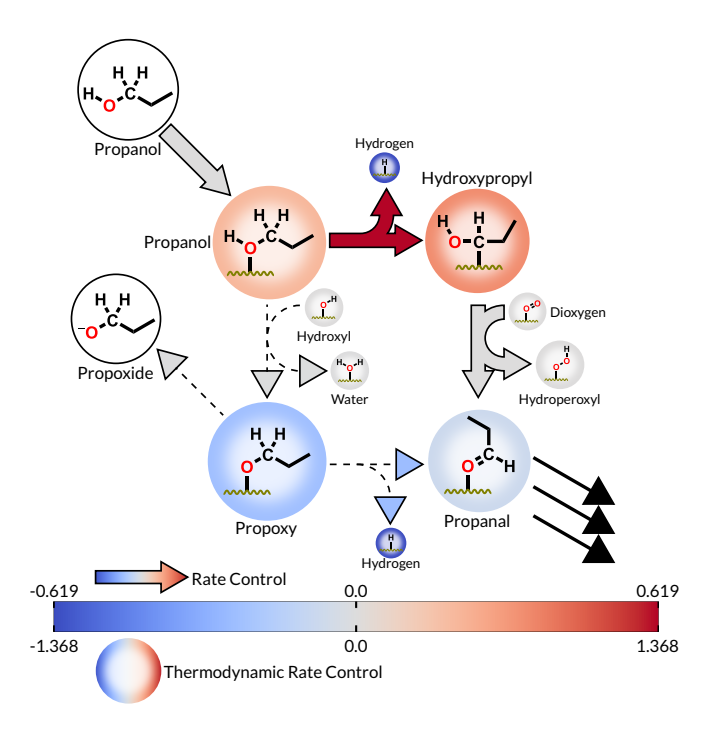


Figure 6: Reaction diagram for the catalytic dehydrogenation of propanol to propanal. For this and all following reaction diagrams, arrow stem thickness represents relative steady state flux and color represents the sensitivity of the rate of methyl propionate formation to the binding energy of intermediates (circles) and reaction rate constants (arrows).

catalyst, while under steady-state conditions this nearly doubles to  $0.25\,\mathrm{eV}$ . This increase in endothermicity of the reaction is coupled with an increase in barrier from  $0.74\,\mathrm{eV}$  under pristine to  $0.81\,\mathrm{eV}$  under steady state conditions. We find no barrier for the reaction of hydroxypropyl with either O or  $\mathrm{O}_2$ . In comparison, the dehydrogenation of propoxy to propanal proceeds over a barrier of  $0.27\,\mathrm{eV}$  ( $0.36\,\mathrm{eV}$ ) under steady-state (pristine) conditions.

One might wonder why the reaction proceeds through the hydroxypropyl intermediate at all, given the presence of propoxide in solution and the lower barrier to dehydrogenation of propoxy to propanal. However, the degree of thermodynamic rate control of adsorbed propoxy is negative, indicating that stabilization of propoxy hinders formation of methyl propionate. In fact, we observe a net desorption of propoxide from the surface following deprotonation of propanol by OH. These observations can be explained by the critical role of hydroxypropyl for the reduction of  $O_2$  to OOH. As we will discuss in a later section, direct abstraction of surface-bound H by  $O_2$  has a substantial barrier, whereas reaction of

the hydroxypropyl intermediate with  $O_2$  to form propanal and OOH is barrierless. The pathway in which proposide anions adsorb to the catalyst and become dehydrogenated to propanal completely bypasses the hydroxypropyl intermediate, thereby inhibiting crucial  $O_2$  reduction to OOH.

Note that the predominant pathway predicted by our microkinetic model for dehydrogenation of propanol to propanal differs from the pathways proposed by Hibbitts and Neurock for dehydrogenation of ethanol to acetaldehyde, despite the similar energetics of these two systems. Hibbitts and Neurock predict that under basic conditions, the alcohol will primarily adsorb to the catalyst as the deprotonated alkoxide, which is in disagreement with the results of our microkinetic model. Our results can be explained both by the unfavorable thermodynamics of adsorption of the alkoxide due to the negative steady-state charge acquired by the catalyst under working conditions, and by the critical role played by the hydroxypropyl intermediate in reduction of O<sub>2</sub>. These factors are difficult to predict in the absence of kinetic modeling.

#### 3.2.2 Dehydrogenation and esterification of propanal to methyl propionate

Subsequent esterification of propanal can proceed through one of two potential pathways, both involving one C-O bond formation step and one C-H bond cleavage step. The most direct pathway proceeds through dehydrogenation of surface-bound propanal to the propanoyl intermediate, which reacts with surface-bound methoxy to form the ester. The alternative pathway involves desorption of propanal, which reacts with methoxide in solution to form a deprotonated hemiacetal anion. The deprotonated hemiacetal anion then adsorbs to the catalyst and undergoes  $\beta$ -hydride elimination to the final ester product. In both pathways, one H atom is deposited onto the catalyst surface and one anion - either methoxide or the deprotonated hemiacetal anion - adsorbs to the surface.

Based on the results of our microkinetic model, we find that both pathways are feasible and contribute to the overall catalyst activity (see Figure 7). A slight majority (53%) of

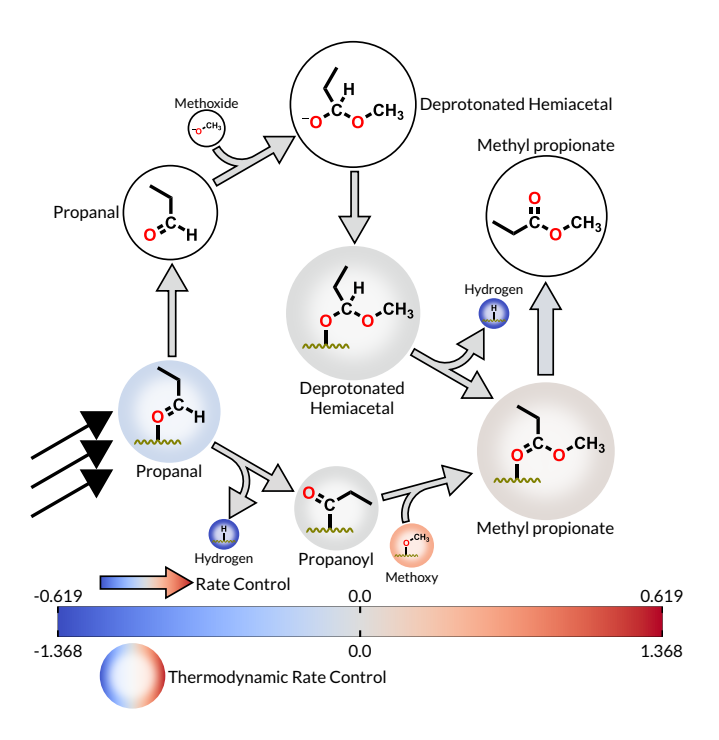


Figure 7: Reaction diagram for the formation of methyl propionate from propanal and methanol.

the propanal that is formed on the catalyst desorbs and proceeds through the hemiacetal pathway, while the remaining propanal (47%) becomes dehydrogenated to propanoyl. Sensitivity analysis shows that the rate of methyl propionate formation is largely unaffected by the kinetic parameters of either pathway, suggesting that esterification of propanal is not rate determining and that both pathways are capable of rapidly converting propanal to methyl propionate, which is consistent with the lack of an observed build up of aldehyde intermediates in the esterification of other primary alcohols.<sup>9</sup>

Note that we do not see any substantial formation of the neutral hemiacetal species either in solution or on the catalyst surface, and solution-phase deprotonated hemiacetal rapidly adsorbs to the catalyst surface and is dehydrogenated to methyl propionate. Similarly, any propanoyl that is formed on the surface reacts exothermically  $(-1.69 \,\mathrm{eV})$  and with modest barrier  $(0.08 \,\mathrm{eV})$  with adsorbed methoxy to form the ester.

#### 3.2.3 The role of hydrogen

The catalyst surface is substantially H-covered in the steady state, with 74% of all active sites occupied by H atoms. This is consistent with experimental working catalyst potential measurements which show that even in oxygen-rich environments, PGM dehydrogenation catalysts tend to become reduced relative to the air-exposed resting catalyst when exposed to dehydrogenation targets such as alcohols. These surface H atoms are byproducts of the dehydrogenation steps involved in the conversion of propanol to methyl propionate and must be removed in order to regenerate the catalyst under steady-state conditions. While it is known that surface-bound H ultimately reduces O<sub>2</sub> to H<sub>2</sub>O, the mechanism by which H is removed from the surface is complex.

Three H atoms are removed from propanol over the course of the reaction: one from an O-H bond and two from C-H bonds. We find that surface-bound oxygen species such as O, OH, and O<sub>2</sub> can facilitate O-H bond scission both by stabilizing the products and lowering or eliminating the reaction barrier, but these oxygen species cannot facilitate C-H bond scission. As such, while O-H bond scission does not necessarily contribute to the overall surface H coverage, the remaining two C-H dehydrogenation steps must necessarily contribute to overall surface H coverage.

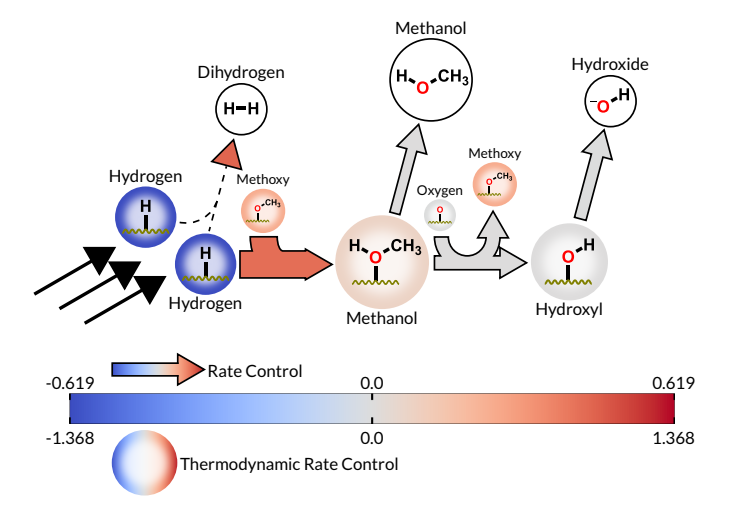


Figure 8: Reaction diagram of the mechanism by which adsorbed H is removed from the catalyst surface.

Once an H atom becomes adsorbed to the catalyst, there are several pathways by which it can be removed. The most direct pathway is desorption of  $H_2$ , though the rate of this pathway is expected to be small, as it does not contribute to the reduction of  $O_2$  and it is not observed to be a major product experimentally. The majority of surface-bound H will react to eventually form  $H_2O$ . However, direct abstraction of H from the catalyst surface by  $O_2$ ,  $O_2$ , or OH are found to have very large barriers. Instead, we find that methoxide adsorbs to the catalyst and abstracts a proton, then it either desorbs as methanol or subsequently reacts with surface-bound O or OH to form OH or  $H_2O$  (see Figure 8). Any OH that is formed rapidly picks up an electron from the catalyst surface and desorbs as  $OH^-$ , which can in turn abstract a proton from the methanol solvent to form  $H_2O$  and regenerate methoxide. In this way, methoxide shuttles H atoms off the surface and onto oxygen, which is less able to directly abstract H from the surface itself,

$$CH_3O^- + 2H* + O* \longrightarrow CH_3OH + OH^- \longrightarrow CH_3O^- + H_2O.$$
 (5)

We find that H has the most strongly negative degree of thermodynamic rate control of all species in the reaction network, with  $\chi_{TRC} = -1.37$ . As such, the presence of H on the catalyst surface strongly suppresses catalytic activity.

However, the negative degree of rate control observed for H does not necessarily arise from catalyst poisoning via site blocking, as around 7% of the catalyst surface remains unoccupied in the steady state. Instead, we find that the presence of H destabilizes co-adsorbates through lateral interactions. Indeed, the high H coverage of the catalyst surface raises the binding energy of other adsorbates by as much as  $0.83\,\mathrm{eV}$  in the steady state (in the case of the deprotonated hemiacetal intermediate). We find that all adsorbates are destabilized under high H coverage conditions, but closed-shell and physisorbed molecules are destabilized to much lesser extent than open-shell reaction intermediates. For example, OOH is destabilized to a much greater extent than adsorbed  $O_2$ , and consequently reduction of  $O_2$  to OOH is

less exothermic under steady state vs. pristine conditions.

#### 3.2.4 The role of oxygen

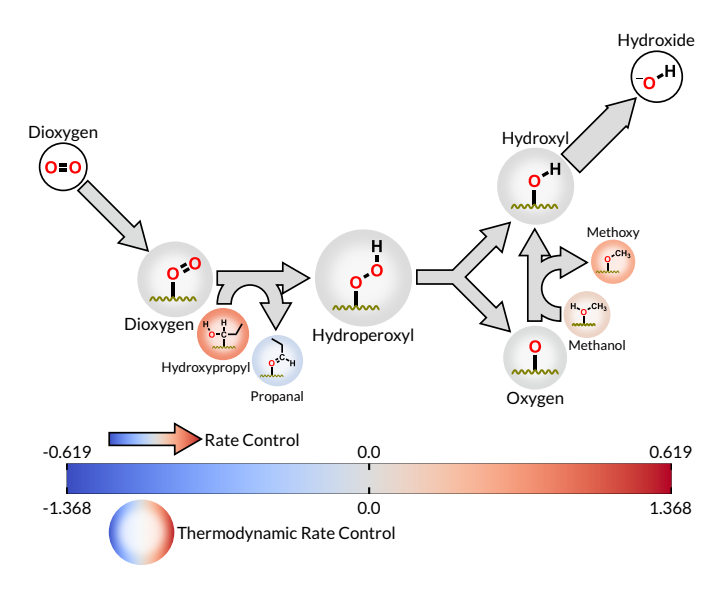


Figure 9: Reaction diagram for the reduction of  $O_2$  to  $OH^-$  on the catalyst.

The influence of  $O_2$  on the dehydrogenation and esterification of propanol to methyl propionate is not straightforward. Clearly  $O_2$  is required for the reaction to occur – the ultimate fate of surface-bound H atoms is  $H_2O$  – but the exact mechanism by which  $O_2$  assists the reaction is not obvious. The most direct pathway to  $O_2$  reduction involves direct abstraction of surface H atoms; however, we find that this reaction occurs only very slowly due its large free energy barrier of 0.77 eV. Other mechanisms by which  $O_2$  can be reduced to OOH involve direct H abstraction from O–H groups on coadsorbates such as propanol and methanol. We find that these reactions are barrierless in all cases, but slightly less thermodynamically favorable than unassisted O–H bond cleavage onto the catalyst surface. In our microkinetic model, we find that only the hydroxypropyl intermediate directly reacts with  $O_2$  to form OOH (see Figure 9). This is likely because of all O–H bond scission steps in the microkinetic model, dehydrogenation of hydroxypropyl to propanal is the only one that is intrinsically exothermic, allowing it to drive the formation of OOH. The exothermicity of this reaction is due to the formation of the stable, closed-shell propanal intermediate,

whereas dehydrogenation of propanol or methanol produces less stable open-shell alkoxy intermediates.

Once OOH is formed on the surface, it rapidly decomposes to O and OH. We find that most OH that forms on the surface rapidly accepts an electron from the catalyst and desorbs as OH<sup>-</sup>. A small amount of OH reacts with propanol to form propoxy and H<sub>2</sub>O, which then desorbs. The remaining O atom must abstract at least one more H atom before desorbing from the surface as OH<sup>-</sup> or H<sub>2</sub>O. However, as with O<sub>2</sub>, direct abstraction of surface H by O has a large free energy barrier (0.73 eV). However, O is also capable of abstracting H atoms directly from the O-H groups of coadsorbates, but unlike O<sub>2</sub>, this reaction is intrinsically exothermic. We find that O primarily reacts with adsorbed methanol to form OH and methoxy.

#### 3.2.5 The role of base

The impact of base in esterification of propanol to methyl propionate is also complex. Ultimately, we find that base facilitates removal of H atoms from the catalyst surface, but that its ability to do so is limited by removal of excess negative charge from the catalyst via OH<sup>-</sup> desorption.

Based on the results of our microkinetic model (see Figure 10), we find that for each methyl propionate produced, approximately 1.64 OH<sup>-</sup> anions and 0.08 propoxide anions desorb from the catalyst surface. To maintain charge balance, 1.19 methoxide anions and 0.53 deprotonated hemiacetal anions adsorb to the catalyst surface. Both methoxide and the deprotonated hemiacetal anions are directly involved in the formation of methyl propionate, but we find that adsorption of methoxide is in excess of what is required to react with propanoyl on the surface to form methyl propionate. This excess methoxide eventually desorbs from the catalyst surface as methanol, thereby facilitating the removal of H atoms. In fact, the effect of base can be broadly characterized as lowering the steady state H atom concentration on the surface, either by direct H atom removal (see equation 5) or by elimi-

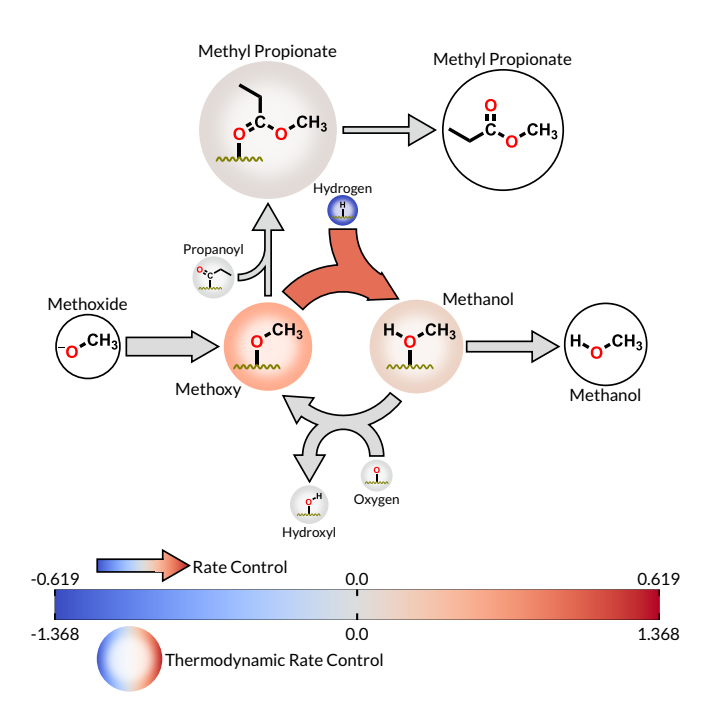


Figure 10: Reaction diagram illustrating the mechanism by which methoxide removes H atoms from the catalyst surface.

nating the need for on-surface O—H bond scission. In the absence of base, it becomes much more difficult to remove excess H from the catalyst surface, which slows the overall reaction due to destabilization of reaction intermediates, as discussed previously. Additionally, as OH cannot desorb as OH<sup>-</sup> in the absence of base, it must further react on the surface to form H<sub>2</sub>O before desorbing.

While base is clearly very effective at scouring H atoms from the catalyst surface, the rate at which this occurs is limited by removal of excess negative charge from the catalyst. On a pristine and uncharged catalyst surface, adsorption of anions from solution is strongly exothermic, due to the large work function of Pd. When an anion adsorbs to the catalyst surface from solution, its excess electron is deposited into the catalyst, making adsorption of subsequent anions less favorable due to the electrostatic repulsion between excess surface electrons. Under steady state conditions, the charge of the catalyst does not change, and thus any anions that adsorb to the catalyst will be exactly balanced by desorption of other anions. The primary way that negative charge is removed from the catalyst is by desorption

of  $OH^-$ , which is formed following reduction of  $O_2$  to OOH. Therefore, we argue that the ability of catalytic base to remove excess H from the catalyst surface is limited by the rate at which  $O_2$  is reduced to OOH.

We observe that the majority of OH formed on the catalyst surface immediately accepts an electron from the catalyst and desorbs as  $\mathrm{OH}^-$ . In the absence of base, OH would need to be further reduced to  $\mathrm{H}_2\mathrm{O}$  before desorbing. While this reaction is strongly exothermic, it has a fairly high free energy barrier of 0.59 eV in the steady state under basic conditions. Consequently, this reaction would compete with O and  $\mathrm{O}_2$  for the limited number of O–H group containing coadsorbates.

In summary, catalytic base plays three key roles in the esterification of propanol on Pd(111): 1) scavenging of H from the catalyst surface, 2) deprotonation of alcohols in solution to the corresponding alkoxide (thereby removing the need for on-surface alcohol deprotonation), and 3) driving surface-bound OH to desorb as  $OH^-$  rather than requiring it be fully hydrogenated to  $H_2O$  on the catalyst.

## 4 Concluding remarks

Our first-principles microkinetic model of the solution-phase base-catalyzed oxidative esterification of propanol to methyl propionate predicts a TOF of 88.4 h<sup>-1</sup>, consistent with the modest experimentally observed activity of the unpromoted catalyst. Sensitivity analysis demonstrates that activity is limited by the slow removal of H from the catalyst surface. Nonetheless, approximately 7% of the catalyst surface is unoccupied in the steady state, suggesting the surface is not necessarily poisoned via site blocking. Rather, we find that the presence of adsorbed H destabilizes other reaction intermediates via strong lateral interactions. Additionally, the activity of the catalyst is hindered by a high kinetic barrier for initial C-H bond scission in propanol and the unfavorable thermodynamics of reduction of O<sub>2</sub> to OOH.

There have been a number of hypotheses for the mechanism by which main group promoter elements improve catalyst activity and selectivity for oxidative dehydrogenation and esterification of alcohols. These hypotheses fall into one of three broad classes: 1) the promoter blocks sites, thereby preventing the formation of strongly-bound undesired side-products (the so-called ensemble effect); <sup>15,16</sup> 2) the promoter indirectly modulates the activity of the catalyst, which can, for example, prevent corrosion <sup>14</sup> or suppress a buildup of H; <sup>13</sup> or 3) the promoter directly interacts with surface adsorbates, either acting as a co-catalyst, <sup>11</sup> or by simply coordinating adsorbates to create more stable configurations. <sup>12</sup>

The results of our microkinetic model and some preliminary calculations on model maingroup promoted surfaces suggest that both the indirect modulation of intrinsic Pd metal binding energetics and direct participation of main group promoter elements may play a role in the oxidative dehydrogenation and esterification of alcohols on Pd. In our microkinetic model, the surface is heavily H-covered, and this results in the destabilization of many reaction intermediates due to repulsive lateral interactions. Preliminary calculations of a Te-promoted Pd(111) surface indicate that most species, including H, bind more weakly to this surface than to the unpromoted surface. We also find that stable molecules and H do not bind to Te atoms at all, whereas other reaction intermediates do (albeit more weakly than to Pd). While in our model the surface is not poisoned by H, it is approximately 74% covered by H, and this yields a strong destabilizing effect on other adsorbates. Consequently, we believe that the Te-promoted catalyst surface will have a substantially lower steady state H coverage than the unpromoted catalyst. Microkinetic analysis of the esterification of propanol to methyl propionate on the Te- and Bi-promoted Pd(111) surfaces will be the subject of a future communication.

# 5 Supporting information

A free energy profile of two representative mechanisms for the overall esterification of 1-propanol to methyl propionate; free energy profiles for they propoxy and hydroxypropyl pathways for propanal formation on the pristine surface; a table of all reaction free energies and free energy barriers for all reactions considered in this model on the pristine surface and under steady state conditions; a table comparing our results to those of Hibbitts and Neurock; steady state rate and degree of rate control for all reactions considered in this model; further details on our double layer capacitor model; details on the calculation of free energies of species in the model; details on the calculation of rate constants; a brief explanation on the differences between our sensitivity analysis and the method described by Campbell; VASP POSCAR files for each species considered in this work; input files to be used with Micki (available on our website).

# 6 Acknowledgments

This material is based upon work supported by the National Science Foundation under Grant No. CHE-1362136. This work used the Extreme Science and Engineering Discovery Environment (XSEDE), which is supported by National Science Foundation grant number TG-CHE120088. J.R.S is a Camille Dreyfus Teacher-Scholar.

## References

- (1) Sheldon, R. Metal-Catalyzed Oxidations of Organic Compounds: Mechanistic Principles and Synthetic Methodology Including Biochemical Processes; Elsevier Science, 2012.
- (2) Vinod, C. P.; Wilson, K.; Lee, A. F. J. Chem. Technol. Biotechnol. 2011, 86, 161–171.
- (3) Parmeggiani, C.; Cardona, F. Green Chem. 2012, 14, 547.

- (4) Mallat, T.; Baiker, A. Chem. Rev. 2004, 104, 3037–3058.
- (5) Sheldon, R. A.; Arends, I.; Dijksman, A. Catal. Today 2000, 57, 157–166.
- (6) Fiege, H.; Wedemeyer, K. Angew. Chem. 1981, 93, 812–813.
- (7) Mallat, T.; Bodnar, Z.; Baiker, A. Stud. Surf. Sci. Catal. 1993, 78, 377–384.
- (8) Mallat, T.; Bodnar, Z.; Baiker, A.; Greis, O.; Strübig, H.; Reller, A. J. Catal. 1993, 142, 237–253.
- (9) Mannel, D. S.; Ahmed, M. S.; Root, T. W.; Stahl, S. S. J. Am. Chem. Soc. 2017, 139, 1690–1698.
- (10) Mallat, T.; Baiker, A. Catal. Today **1994**, 19, 247–284.
- (11) Furuya, N.; Motoo, S. J. Electroanal. Chem. 1979, 98, 195–202.
- (12) Smits, P. C. C.; Kuster, B. F. M.; van der Wiele, K.; van der Baan, S. Appl. Catal. 1987, 33, 83–96.
- (13) Parsons, R.; VanderNoot, T. J. Electroanal. Chem. Interfacial Electrochem. 1988, 257, 9-45.
- (14) Tsujino, T.; Ohigashi, S.; Sugiyama, S.; Kawashiro, K.; Hayashi, H. *J. Mol. Catal.* **1992**, 71, 25–35.
- (15) Kimura, H.; Tsuto, K.; Wakisaka, T.; Kazumi, Y.; Inaya, Y. Appl. Catal., A 1993, 96, 217–228.
- (16) Mallat, T.; Bodnar, Z.; Baiker, A. ACS Symp. Ser. 1993, 523, 308–317.
- (17) Horányi, G.; Vértes, G.; König, P. Acta Chim. Acad. Sci. Hung. 1972, 72, 179–187.
- (18) Dirkx, J. M. H.; van der Baan, H. S.; van den Broek, J. M. A. J. J. *Carbohydr. Res.* **1977**, *59*, 63–72.

- (19) Dirkx, J. M. H.; van der Baan, H. S. J. Catal. 1981, 67, 14-20.
- (20) Dijkgraaf, P. J. M.; Duisters, H. A. M.; Kuster, B. F. M.; van der Wiele, K. J. Catal. 1988, 112, 337–344.
- (21) Nicoletti, J. W.; Whitesides, G. M. J. Phys. Chem. 1989, 93, 759-767.
- (22) Grunwaldt, J.-D.; Caravati, M.; Baiker, A. J. Phys. Chem. B 2006, 110, 25586–25589.
- (23) Hoffman, A.; Kuhn, A. T. *Electrochim. Acta* **1964**, *9*, 835–839.
- (24) Dijkgraaf, P. J. M.; Rijk, M. J. M.; Meuldijk, J.; van der Wiele, K. J. Catal. 1988, 112, 329–336.
- (25) Dijkgraaf, P. J. M. Oxidation of Glucose to Glucaric Acid by Pt/C Catalysts. Ph.D. thesis, Technische Universiteit Eindhoven, 1989.
- (26) Vinke, P.; de Wit, D.; de Goede, A. T. J. W.; van Bekkum, H. *Stud. Surf. Sci. Catal.* **1992**, 72, 1–20.
- (27) DiCosimo, R.; Whitesides, G. J. Phys. Chem. 1989, 93, 768–775.
- (28) Schuurman, Y.; Kuster, B.; van der Wiele, K.; Marin, G. *Stud. Surf. Sci. Catal.* **1992**, 72, 43–55.
- (29) Vassilyev, Y. B.; Khazova, O. A.; Nikolaeva, N. N. J. Electroanal. Chem. **1985**, 196, 127–144.
- (30) Popović, K. D.; Marković, N. M.; Tripković, A. V.; Adžić, R. R. J. Electroanal. Chem. **1991**, 313, 181–199.
- (31) Adkins, H.; Broderick, A. E. J. Am. Chem. Soc. **1928**, 50, 499–503.
- (32) Lauder, I. Trans. Faraday Soc. **1948**, 44, 729–735.
- (33) McKenna, F. E.; Tartar, H. V.; Lingafelter, E. C. J. Am. Chem. Soc. 1953, 75, 604–607.

- (34) Powell, A. B.; Stahl, S. S. Org. Lett. 2013, 15, 5072-5075.
- (35) Hibbitts, D. D.; Neurock, M. J. Catal. **2013**, 299, 261–271.
- (36) Kresse, G.; Hafner, J. Phys. Rev. B **1993**, 47, 558–561.
- (37) Kresse, G.; Hafner, J. Phys. Rev. B **1994**, 49, 14251–14269.
- (38) Kresse, G.; Furthmüller, J. Phys. Rev. B 1996, 54, 11169–11186.
- (39) Kresse, G.; Furthmüller, J. Comput. Mater. Sci **1996**, 6, 15–50.
- (40) Larsen, A. H.; Mortensen, J. J.; Blomqvist, J.; Castelli, I. E.; Christensen, R.; Dułak, M.; Friis, J.; Groves, M. N.; Hammer, B.; Hargus, C.; Hermes, E. D.; Jennings, P. C.; Jensen, P. B.; Kermode, J.; Kitchin, J. R.; Kolsbjerg, E. L.; Kubal, J.; Kaasbjerg, K.; Lysgaard, S.; Maronsson, J. B.; Maxson, T.; Olsen, T.; Pastewka, L.; Peterson, A.; Rostgaard, C.; Schiøtz, J.; Schütt, O.; Strange, M.; Thygesen, K.; Vegge, T.; Vilhelmsen, L.; Walter, M.; Zeng, Z.; Jacobsen, K. W. J. Phys.: Condens. Matter 2017, 29, 273002.
- (41) Perdew, J. P.; Burke, K.; Ernzerhof, M. Phys. Rev. Lett. 1996, 77, 3865–3868.
- (42) Perdew, J. P.; Burke, K.; Ernzerhof, M. Phys. Rev. Lett. 1997, 78, 1396.
- (43) Heyd, J.; Scuseria, G. E. J. Chem. Phys. **2004**, 121, 1187–1192.
- (44) Heyd, J.; Peralta, J. E.; Scuseria, G. E.; Martin, R. L. J. Chem. Phys. 2005, 123, 174101.
- (45) Heyden, A.; Bell, A. T.; Keil, F. J. J. Chem. Phys. **2005**, 123, 224101.
- (46) Izmaylov, A. F.; Scuseria, G. E.; Frisch, M. J. J. Chem. Phys. **2006**, 125, 0–8.
- (47) Heyd, J.; Scuseria, G. E.; Ernzerhof, M. J. Chem. Phys. **2006**, 124, 219906.

- (48) Krukau, A. V.; Vydrov, O. A.; Izmaylov, A. F.; Scuseria, G. E. J. Chem. Phys. 2006, 125, 224106.
- (49) Grimme, S.; Antony, J.; Ehrlich, S.; Krieg, H. J. Chem. Phys. **2010**, 132, 154104.
- (50) Grimme, S.; Ehrlich, S.; Goerigk, L. J. Comput. Chem. 2011, 1456–1465.
- (51) Moellmann, J.; Grimme, S. J. Phys. Chem. C **2014**, 118, 7615–7621.
- (52) Gil, A.; Clotet, A.; Ricart, J. M.; Kresse, G.; García-Hernández, M.; Rösch, N.; Sautet, P. Surf. Sci. **2003**, 530, 71–86.
- (53) Zeng, Z.; Greeley, J. Catal. Commun. **2014**, 52, 78–83.
- (54) Zhao, Z. J.; Li, Z.; Cui, Y.; Zhu, H.; Schneider, W. F.; Delgass, W. N.; Ribeiro, F.; Greeley, J. J. Catal. 2017, 345, 157–169.
- (55) Gale, W.; Totemeier, T. Smithells Metals Reference Book; Elsevier Science, 2003.
- (56) Monkhorst, H. J.; Pack, J. D. Phys. Rev. B 1976, 13, 5188-5192.
- (57) Gunceler, D.; Letchworth-Weaver, K.; Sundararaman, R.; Schwarz, K. A.; Arias, T. A. Modell. Simul. Mater. Sci. Eng. 2013, 21, 074005.
- (58) Mathew, K.; Sundararaman, R.; Letchworth-Weaver, K.; Arias, T. A.; Hennig, R. G. J. Chem. Phys. 2014, 140.
- (59) Mathew, K.; Hennig, R. G. Implicit self-consistent description of electrolyte in plane-wave density-functional theory. 2016; http://arxiv.org/abs/1601.03346, arXiv:1601.03346. arXiv.org e-Print archive.
- (60) Jónsson, H.; Mills, G.; Jacobsen, K. W. In Classical and Quantum Dynamics in Condensed Phase Simulations; Berne, B. J., Ciccotti, G., Coker, D. F., Eds.; World Scientific, 1998; Chapter 16, pp 385–404.

- (61) Henkelman, G.; Jónsson, H. J. Chem. Phys. 2000, 113, 9978–9985.
- (62) Sheppard, D.; Terrell, R.; Henkelman, G. J. Chem. Phys. 2008, 128, 134106.
- (63) Henkelman, G.; Jónsson, H. J. Chem. Phys. **1999**, 111, 7010.
- (64) Kästner, J.; Sherwood, P. J. Chem. Phys. 2008, 128, 014106.
- (65) Frisch, M. J.; Trucks, G. W.; Schlegel, H. B.; Scuseria, G. E.; Robb, M. A.; Cheeseman, J. R.; Scalmani, G.; Barone, V.; Mennucci, B.; Petersson, G. A.; Nakatsuji, H.; Caricato, M.; Li, X.; Hratchian, H. P.; Izmaylov, A. F.; Bloino, J.; Zheng, G.; Sonnenberg, J. L.; Hada, M.; Ehara, M.; Toyota, K.; Fukuda, R.; Hasegawa, J.; Ishida, M.; Nakajima, T.; Honda, Y.; Kitao, O.; Nakai, H.; Vreven, T.; Montgomery Jr., J. A.; Peralta, J. E.; Ogliaro, F.; Bearpark, M.; Heyd, J. J.; Brothers, E.; Kudin, K. N.; Staroverov, V. N.; Keith, T.; Kobayashi, R.; Normand, J.; Raghavachari, K.; Rendell, A.; Burant, J. C.; Iyengar, S. S.; Tomasi, J.; Cossi, M.; Rega, N.; Millam, J. M.; Klene, M.; Knox, J. E.; Cross, J. B.; Bakken, V.; Adamo, C.; Jaramillo, J.; Gomperts, R.; Stratmann, R. E.; Yazyev, O.; Austin, A. J.; Cammi, R.; Pomelli, C.; Ochterski, J. W.; Martin, R. L.; Morokuma, K.; Zakrzewski, V. G.; Voth, G. A.; Salvador, P.; Dannenberg, J. J.; Dapprich, S.; Daniels, A. D.; Farkas, O.; Foresman, J. B.; Ortiz, J. V.; Cioslowski, J.; Fox, D. J. Gaussian Op Revision D.01. Gaussian Inc. Wallingford CT 2016.
- (66) Dunning Jr, T. H. J. Chem. Phys. 1989, 90, 1007.
- (67) Marenich, A. V.; Cramer, C. J.; Truhlar, D. G. J. Phys. Chem. B **2009**, 113, 6378–6396.
- (68) Hermes, E. D.; Janes, A. N.; Schmidt, J. R. unpublished work.
- (69) Hansen, H. A.; Viswanathan, V.; Nørskov, J. K. J. Phys. Chem. C 2014, 118, 6706–6718.
- (70) Silbaugh, T. L.; Campbell, C. T. J. Phys. Chem. C 2016, 25161–25172.

- (71) Campbell, C. T. Top. Catal. 1994, 1, 353–366.
- (72) Stegelmann, C.; Andreasen, A.; Campbell, C. T. J. Am. Chem. Soc. 2009, 131, 8077–8082.
- (73) Campbell, C. T. ACS Catal. 2017, 7, 2770–2779.

